TRANSACTIONS ON ELECTRICAL AND ELECTRONIC MATERIALS
Vol. 17, No. 5, pp. 270-274, October 25, 2016

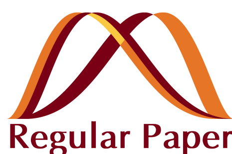

pISSN: 1229-7607 eISSN: 2092-7592
DOI: http://dx.doi.org/10.4313/TEEM.2016.17.5.270
OAK Central: http://central.oak.go.kr

Control of Short-Channel Effects in Nano DG MOSFET Using Gaussian-Channel Doping Profile

Morteza Charmi†
Department of Nano Physics, Malek-Ashtar University of Technology, Shahinshahr, Iran

Received January 11, 2016; Revised July 14, 2016; Accepted July 14, 2016

This article investigates the use of the Gaussian-channel doping profile for the control of the short-channel effects in the double-gate MOSFET whereby a two-dimensional (2D) quantum simulation was used. The simulations were completed through a self-consistent solving of the 2D Poisson equation and the Schrodinger equation within the non-equilibrium Green's function (NEGF) formalism. The impacts of the p-type-channel Gaussian-doping profile parameters such as the peak doping concentration and the straggle parameter were studied in terms of the drain current, on-current, off-current, sub-threshold swing (SS), and drain-induced barrier lowering (DIBL). The simulation results show that the short-channel effects were improved in correspondence with incremental changes of the straggle parameter and the peak doping concentration.

Keywords: Short-channel effects, Non-equilibrium Green's function, Gaussian-channel doping profile, Straggle parameter

1. INTRODUCTION

Metal-oxide semiconductor field-effect transistors (MOSFETs) constitute the basic building block of present-day CMOS technology. The current research in this field is largely geared toward an increasing of the device density through an aggressive scaling of the device-feature sizes [1], and an improvement of the MOSFET-structure performances such as those of the double-gate (DG) MOSFETs [2-4], nano-wire FETs [5-7], nanoscale FinFETs [8,9], and nano-tube transistors [10]. As the channel length of the MOSFETs continues to shrink to several tens of nanometers, the source-to-drain and gate-tunneling of these near-ballistic devices and the inversion layers that are of a several-nanometer thickness, which are in the MOSFETs, become important issues [11].

The gate-tunneling in the MOSFETs can be reduced with the use of the high-k gate dielectric [12-14], while in a MOSFET with a channel length of approximately 10 nm, the off-current is a salient value that leads to an increase of the sub-threshold swing (SS) and a lowering of both the drain-induced barrier and the threshold voltage. One of the parameters that improves the short-channel effects and controls the threshold voltage is the channel-doping concentration; for this reason, researchers often apply channel doping of a uniform concentration to control the short-channel effects in MOSFETs [15-18]; moreover, it must be noted that the nature of the actual in-practice transistor-channel doping profile becomes closer to that of the Gaussian profile due to the ion-implantation stages that are required during the fabrication process [19-21]. For this article, the Gaussian-channel doping profile that is used to control the short-channel effects in the DG MOSFET are therefore investigated with the use of a two-dimensional (2D) quantum simulation, whereby the MOSFET-channel length is 9 nm and the MOSFET-channel thickness is 3 nm. For the simulations, the 2D Poisson equation and the Schrodinger equation were self-consistently solved with open-boundary conditions within the non-equilibrium Green's function (NEGF) formalism.

† Author to whom all correspondence should be addressed:
E-mail: charmi@guilan.ac.ir, charmi.phy@gmail.com

Copyright ©2016 KIEEME. All rights reserved.
This is an open-access article distributed under the terms of the Creative Commons Attribution Non-Commercial License (http://creativecommons.org/licenses/by-nc/3.0) which permits unrestricted noncommercial use, distribution, and reproduction in any medium, provided the original work is properly cited.

2. DEVICE STRUCTURE

Figure 1 shows the schematic of the symmetric DG MOSFETs

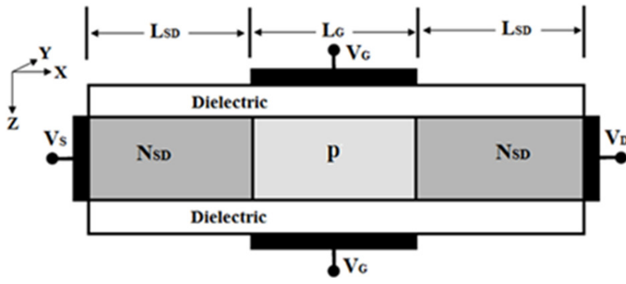

Fig. 1. Ultra-thin-body DG-MOSFET structure.

Table 1. Parameters for DG-MOSFET structure that was used in the simulation.

Device parameters	Value
Channel thickness: T_{Ch} [nm]	3
Effective oxide thickness: EOT [nm]	0.1
Gate length: L_G [nm]	9
Source/Drain length: L_{SD} [nm]	7.5
Source/Drain-doping concentration: N_{SD} [cm^{-3}]	2E20
Power-supply voltage: V_{DD} [V]	0.7
Gate-work function: Φ [eV]	4.480
Ambient temperature: T [K]	300

and the corresponding co-ordinates, where the x-axis is along the channel (transport direction), the z-axis is along the quantum-confinement direction, and the y-dimension is treated as infinite; however, the quantum confinement in the z-direction introduces sub-bands, and for an ultra-thin body, only a few sub-bands are occupied. A short-channel length (L_G = 9 nm), an ultra-thin channel thickness (T_{Ch} = 3 nm), and a highly-doped source/drain contact were all considered. According to the end of the international technology roadmap for semiconductors (ITRS) [1], the off-current is equal to 0.1 μA and the effective oxide thickness (EOT) is equal to 0.5 nm. To produce an EOT = 0.5 nm, a high-k gate dielectric such as HfO_2 for which $k_{high\text{-}k}$=23 and $T_{high\text{-}k}$=3 nm is used. The gate-work function, Φ, meanwhile, is equal to 4.480 eV to obtain I_{off}=0.1 μA/μm, and this gate-work value is a fixed parameter in all of the overdrives in this article. To provide a clear answer regarding the effect of the Gaussian-channel doping profile, the junctions are abrupt and there is no S/D-doping gradient. The structural parameters of the device are presented in Table 1.

3. SIMULATION APPROACH

The 2D ballistic-transport equation in the MOSFET-channel region was solved with the use of the mode-space approach [23], whereby the problem is split into two one-dimensional (1D) problems. In the quantum-confinement direction (z-direction), the Schr?dinger equation was solved to generate the sub-bands. In the transport direction (x-direction), the NEGF approach, which is equivalent to solving the Schr?dinger equation with the open-boundary condition, was used to describe the ballistic quantum transport.

In the vertical direction (z-direction in Fig. 1), the Schrödinger equation was solved for each x-position independently to generate the ith-sub-band profile, E_i (x), and the corresponding wave function, ψ_i (x, z), as follows:

$$-\frac{\hbar^2}{2m_z^*}\frac{\partial^2}{\partial z^2}\psi_i(x,z)-qV(x,z)\psi_i(x,z)=E_i(x)\psi_i(x,z) \quad (1)$$

where m_z^* is the effective mass along the z-direction, q is the electron charge, ħ is the Planck's constant, and V(x, z) is the electrostatic potential [24-26].

For the sub-band, *i*, with the planewave eigenenergy, E_{kj}, the retarded Green's function that is relevant to the 1D transport is written as follows:

$$\begin{aligned} G(E) &= [EI - H[E_i(x), E_{k_j}] - \Sigma_S - \Sigma_D]^{-1} \\ &= [E_l I - H[E_i(x)] - \Sigma_S - \Sigma_D]^{-1} \end{aligned} \quad (2)$$

where Σ_S and Σ_D are the self-energies of the source and drain, respectively, $E_l = E - E_{k_j}$ is the longitudinal energy, *I* is the identity matrix, and H is the Hamiltonian of the mode-space approach for the *i* with the E_{k_j}. The sub-band index, *i*, runs over all of the sub-bands, but the real calculations, including those of the lowest-few sub-bands, provided the desired accuracy. As can be seen from Eq. (2), the assumed transport here is completely ballistic. The spectral-density functions that are due to the source/drain contacts can be obtained from the following equation [24]:

$$A_S = G\Gamma_S G^\dagger \qquad and \qquad A_D = G\Gamma_D G \quad (3)$$

where $\Gamma_S = i(\Sigma_S - \Sigma_S^\dagger)$ and $\Gamma_D = i(\Sigma_D - \Sigma_D^\dagger)$. The source-related spectral function is filled up according to the Fermi energy in the source contact, while the drain-related spectral function is filled up according to the Fermi energy in the drain contact, and the diagonal entries of the spectral functions represent the local density of states (LDOS) at each node [24]. The 2D-electron density is as follows:

$$\begin{aligned} n_{2D}(x) = \sum\nolimits_i \{\int_{-\infty}^{+\infty} dE[F_{-1/2}(\mu_S - E)D_{Si}(E,x) \\ + F_{-1/2}(\mu_D - E)D_{Di}(E,x)]\} \end{aligned} \quad (4)$$

where $F_{-1/2}$ is the Fermi integral of the order - 1/2 [27], μ_S (μ_D) is the source/drain-Fermi level, D_{Si} (*E, x*) is the LDOS of the ith sub-band that is contributed by the source, and D_{Di} (*E, x*) is the LDOS of the ith sub-band that is contributed by the drain, the calculations of which are based on the Green's-function formalism. The total-electron density is the product of n_{2D} (*x*) and $|\psi_i(x, z)|^2$.

In the longitudinal direction, the NEGF approach was used to describe the ballistic quantum transport. A 2D Poisson equation was then solved in the silicon channel and the gate oxide to update the electrostatic potential (a nonlinear Poisson equation was solved to improve the outer-loop convergence [28]). The iteration between the quantum-transport equation and the Poisson equation was repeated until the self-consistency was achieved. Lastly, the source-drain current can be calculated as follows [24]:

$$I_{SD} = \sum\nolimits_i I_{0i} \int_{-\infty}^{+\infty} \left[F_{-1/2}(\mu_S - E) - F_{-1/2}(\mu_D - E)\right] T_{SDi}(E)\, dE \quad (5)$$

where I_{0i} is a constant with the dimension of the current, $F_{-1/2}$ is the Fermi-Dirac integral of the order - 1/2, $\mu_{S/D}$ is the source/drain-Fermi level, the index of *i* is the number of sub-bands, and T_{SDi} is the transmission coefficient from the source to the drain for the *i*th sub-band at the energy, *E*. Accordingly, the following equation (6), is relevant:

$$T(E) = \text{trace}\left(\Gamma_S(E)G(E)\Gamma_D(E)G^\dagger(E)\right) \quad (6)$$

4. RESULTS AND DISCUSSION

This paper presents a systematic study for the optimization of the Gaussian-channel doping parameters that are for the control of the short-channel effects in the double-gate MOSFET. According to Fig. 1, the locations of the x- and z-axes of the 2D structure are along the source-channel interface and the upper-channel oxide interface, respectively. Since the n-channel DG MOSFETs were also analyzed, a Gaussian p-type body was assumed; therefore, N(z) is the Gaussian-vertical doping profile in the p-type channel that can be expressed as follows [14]:

$$N(z) = N_P * \exp\left[-\left(\frac{z-R_P}{\sqrt{2}\sigma_P}\right)^2\right] \tag{11}$$

where N_P is the peak doping concentration at the projected range, R_P, and the straggle, σ_P, and is also the standard deviation of the Gaussian pulse. For all of the overdrives in this article, the projected range of the peak doping, R_P, is at the middle of the channel thickness, and only the values of the N_P and the σ_P are variable. At first, the effect of the N_P was investigated, and this was followed by a studying of the impact of the σ_P is studied.

4.1 Peak doping concentration

In this section, the N_P is varied from 1E15 cm^{-3} to 1E20 cm^{-3}, while the σ_P is maintained at 0.5 nm. The Gaussian-doping profile versus the channel thickness is shown in Fig. 2. Due to the constant σ_P value, the rate of the doping fall from the center of the channel to the ends of the channel for all of the N_P is identical. Figure 3 shows the on-current, off-current, and on-off-current ratios versus the Gaussian-channel doping concentration at $V_{DS} = V_{GS} = 0.7$ V. The range of the channel-doping concentration is from 1E15 cm^{-3} to 1E20 cm^{-3}. It is clear from Fig. 3(a) that the on-current first stays constant at low doping levels and starts to decrease when the doping is sufficiently high. Because the concentration of the channel doping controls the height of the source-to-channel barrier in a fixed-gate voltage, and the electron inversion becomes feeble with the increasing of the p-type channel doping, the barrier height increased so that the on-current was decreased; alternatively, when the body doping is high, the carrier mobility in the channel can be strongly degraded by the dopants, leading to a decrease of the on-current.

In the sub-threshold region, mobile charges can be neglected. The Poisson's equation takes only the fixed charges that are of a p-type concentration. So with an increasing of the channel-doping concentration, the sub-threshold current is decreased so that the off-current is decreased at high doping concentrations, as shown in Fig. 3(b). Heavy body doping also causes a strong band-to-band tunneling from the body to the drain, which can be a significant leakage-current source.

When the fixed gate-work function is used in the MOSFETs, due to the varying of the off-current, the ratio of the on-current to the off-current (I_{on}/I_{off}) becomes a more-important parameter than the on-state current. According to Fig. 3(c), with the increasing of the channel-doping concentration, although both the on-current and the off-current are decreasing at higher doping concentrations, and the rate of the reduction of the off-current is faster than that of the on-current, the on-current/off-current ratio becomes very high at the higher doping concentrations.

Figure 4 shows the drain current versus the gate voltage for different Gaussian-channel doping concentrations at the fixed gate-work function. It is clear that the threshold voltage is increased with the increasing of the doping concentration, and this is because at un-doped or lightly doped levels, the silicon chan-

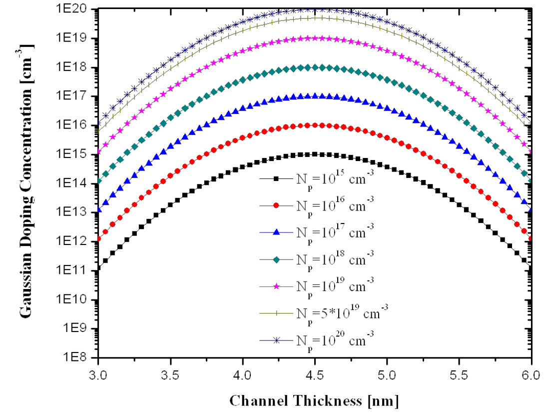

Fig. 2. Gaussian-doping profile versus channel thickness for different peak doping concentrations with fixed straggle parameter.

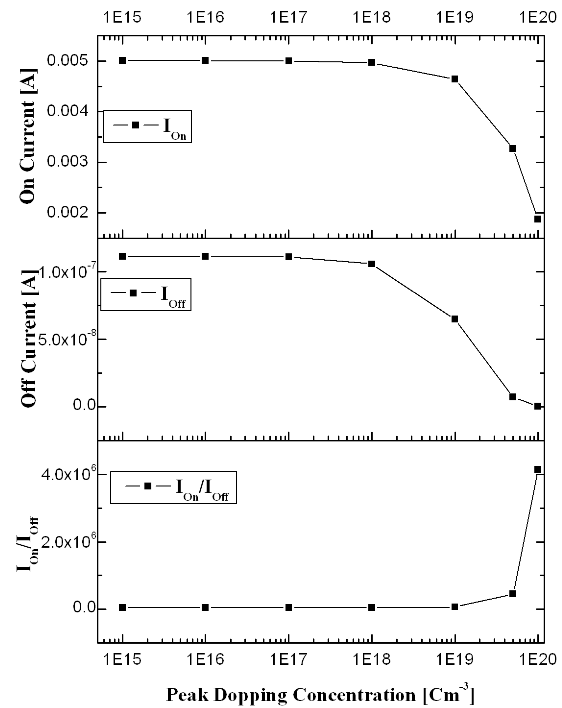

Fig. 3. (a) On-current, (b) off-current, and (c) on-off-current ratios versus peak doping concentration at $V_{DS} = 0.7$ V.

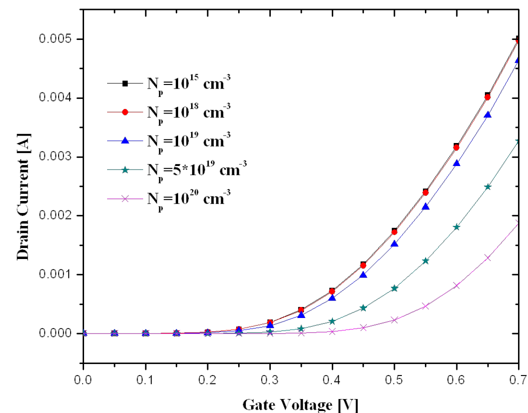

Fig. 4. Drain current versus gate voltage for different peak doping concentrations in linear scale at $V_{DS} = 0.7$ V.

nel is fully depleted and the potential at the center of the channel is not fixed; therefore, the potential inside the channel moves as a whole along with the applied gate voltage in the sub-threshold region. As the doping concentration further increases, the center potential of the silicon film eventually remains unchanged even under large applied gate voltages; in this case, the device becomes partially depleted. Consequently, the threshold voltage is increased, and the SS starts to degrade as the doping level increases, as shown in Fig. 5. In Fig. 5, the SS is plotted for both the uniform doping and the Gaussian doping with a straggle of 0.5 nm. The SS parameter for the uniform doping is more than that for the Gaussian doping at high doping levels because the uniform doping leads to a device that is more partially depleted than that from the Gaussian-doping profile.

Figure 6 illustrates the drain induced barrier lowering (DIBL) versus the channel-doping concentration for the uniform and Gaussian profiles. The DIBL first stays constant at the low doping levels and starts to decrease when the doping is sufficiently high. For the un-doping or light doping in the DG MOSFET, the electric-field lines that emanate from the drain are terminated at the gates; for the high doping levels, the electric-field lines from the drain are drawn toward the center of the channel where they are terminated. The effect of the electric field from the drain on the channel electrostatics for the highly doped p-type DG MOSFET is therefore much smaller than that on the channel electrostatics for the low-doped DG MOSFET; this means that the drain-contact effect on the channel is reduced and the control of the gate on the channel is increased, thereby leading to a decrease of the DIBL when the doping level is increased. Also, for the Gaussian doping that occurs only at the center of the channel, the doping concentration is identical to that of the uniform doping, and the doping is reduced at the ends of the channel thickness. The control of the drain on the channel for the uniform doping is therefore less than that on the channel for the Gaussian doping, and the DIBL of the uniform doping is less than that of the Gaussian doping at high doping concentrations.

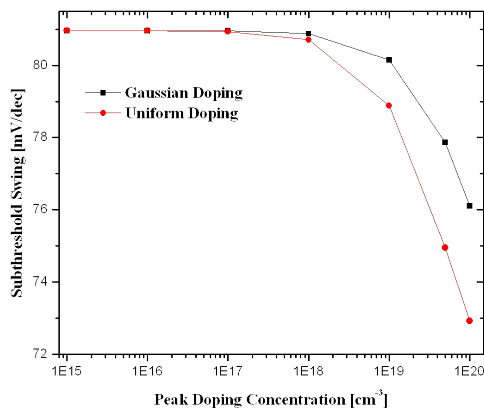

Fig. 5. SS versus channel-doping concentrations for uniform and Gaussian profiles.

4.2 Straggle parameter

In this section, the straggle parameter, σ_P, is varied while the peak doping concentration, N_P, is kept at 5E19 cm^{-3}. Figure 7 shows the Gaussian-doping profile with an N_P = 5E19 cm^{-3} versus the channel thickness for the σ_P=1 nm, 0.5 nm, and 0.1 nm. Clearly, with the decreasing of the σ_P straggle parameter, the doping value is decreased from the center of the channel to the ends of the channel in the gate direction (z-axes). As for the σ_P=0.1 nm, only approximately 0.5 nm of the middle of the channel thickness comprises the net doping concentrations, as the rest of the thickness is undoped. For the σ_P=0.5 nm, the value of the doping concentration at the ends of the channel thickness is decreased to 5E16 cm^{-3} and is relative to the middle of the channel that is 5E19 cm^{-3}. For the σ_P=1 nm, the doping-concentration value at the ends of the channel thickness is decreased to 5E18cm^{-3}, and for the uniform-doping profile, the N_P in the channel of 5E19 cm^{-3} is identical.

The drain current versus the gate voltage for different σ_P values are shown in Fig. 3. With the decreasing of the σ_P straggle parameter, the drain current is increased, and for the uniform channel thickness, the drain-current value is the minimum. Because the reduction of the σ_P results in the decrease of the rate of the doping value from the middle of the channel to the boundary, and the reduction of the channel doping reduces the ionized impurity, an increased channel mobility eventually leads to the increase of both the drain current and the on-current (Table 2). With the decreasing of the σ_P, the doping concentration is decreased, the channel is fully depleted, and the potential at the center of the channel is not fixed, so the threshold voltage is decreased (Fig. 8) and the SS is increased (Table 2).

Table 2 shows the on-current, off-current, and on-off-current ratios, the SS, and the DIBL for the uniform channel doping and the Gaussian doping where the σ_P=1 nm, 0.5 nm, and 0.1 nm. In the sub-threshold region, the Poisson's equation is compatible with only the fixed charges of the p-type concentration, so with the decreasing of the σ_P, the doping concentration is decreased, the band-to-band tunneling from the channel to the drain is

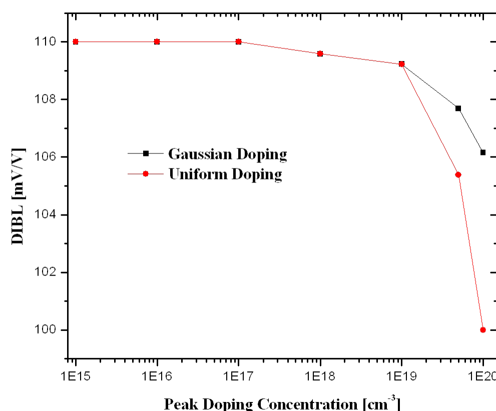

Fig. 6. DIBL versus channel-doping concentrations for uniform and Gaussian profiles.

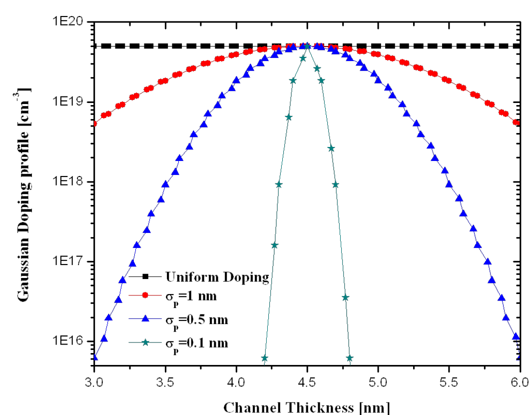

Fig. 7. Gaussian-doping profile versus channel thickness for different straggle parameters with fixed peak doping concentration.

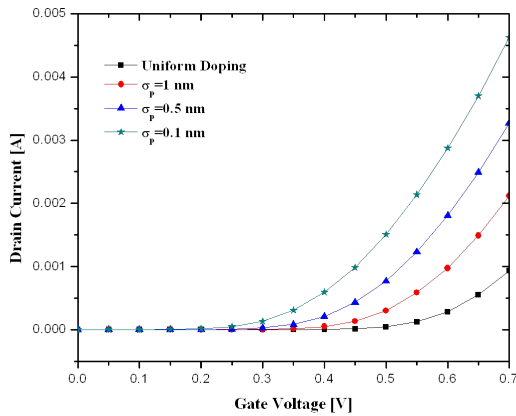

Fig. 8. Drain current versus gate voltage for different straggle parameters in linear scale at V_{DS} = 0.7 V.

Table 2. On-current, off-current, and on-off-current ratios, SS, and DIBL for uniform channel doping and for Gaussian doping with straggle values of σ = 1 nm, 0.5 nm, and 0.1 nm.

Straggle Parameter	I_{On} [A]	I_{Off} [A]	I_{On}/I_{Off}	SS [mV/dec]	DIBL [mV/V]
Uniform Doping	9.30E-04	3.39E-11	2.75E + 07	74.95	106.15
σ_P=1 nm	2.12E-03	7.76E-10	2.73E + 06	76.35	107.69
σ_P=0.5 nm	3.27E-03	7.27E-09	4.49E + 05	77.86	109.23
σ_P=0.1 nm	4.63E-03	6.38E-08	7.25E + 04	80.13	110.00

increased, and the off-current is increased; furthermore, the I_{on}/I_{off} is decreased with the decreasing of the $\sigma_P$straggle parameter. When the σ_P in the Gaussian profile is decreased, the doping concentration is also decreased, whereas the rate of the electric-field lines that emanates from the drain and is terminated at the gates is increased so that the impact of the drain contact on the channel is increased; here, the increase of the drain-contact impact leads to an increase of the DIBL, as shown in Table 2.

5. CONCLUSIONS

A novel approach that involves the straggle parameter and the peak doping concentration of the Gaussian-doping profile in terms of the nano double-gate MOSFETs was studied with the use of a 2D quantum simulation that was performed within the NEGF formalism. The decreasing of the straggle parameter here resulted in the increasing of the SS and the DIBL and the decreasing of the off-current and the threshold voltage. When the doping concentration was increased, the short-channel effects improved, whereby the improvement of the short-channel effects that was caused by the uniform channel doping is more than that of the short-channel effects from the Gaussian channel doping at the same doping concentration.

REFERENCES

[1] International Technology Roadmap for Semiconductor, Available from:/http://public.itrs.net

[2] A. A. Orouji, H. R. Mashayekhi, and M. Charmi, *Mat. Sci. Semicon. Proc.*, **15**, 572 (2012). [DOI: http://dx.doi.org/10.1016/j.mssp.2012.04.011]

[3] M. Charmi, A. A. Orouji, and H. R. Mashayekhi, *Mat. Sci. Semicon. Proc.*, **16**, 311 (2013). [DOI: http://dx.doi.org/10.1016/j.mssp.2012.09.019]

[4] F. Liu, J. He, J. Zhang, Y. Chen, and M. Chan, *IEEE T. Electron Dev.*, **55**, 3494 (2008). [DOI: http://dx.doi.org/10.1109/TED.2008.2006544]

[5] M. Shin, *IEEE T. Nanotechnology*, **6**, 230 (2007). [DOI: http://dx.doi.org/10.1109/TNANO.2007.891819]

[6] S. Bhowmick and K. Alam, *Nano-Micro Letters*, **2**, 83 (2010). [DOI: http://dx.doi.org/10.1007/BF03353623]

[7] J. G. Yun, S. Cho, and B. G. Park, *Solid-State Electronics*, **64**, 42 (2011). [DOI: http://dx.doi.org/10.1016/j.sse.2011.07.003]

[8] J. G. Fossum, M. M. Chowdhury, V. P. Trivedi, T. J. King, Y. K. Choi, J. An, and B. Yu, *IEDM Technical Digest*, 679 (2003).

[9] L. Zhang, C. Ma, J. He, X. Lin, and M. Chan, *Solid-State Electronics*, **54**, 806 (2010). [DOI: http://dx.doi.org/10.1016/j.sse.2010.03.020]

[10] K. Alam and R. Lake, *Appl. Phys. Lett.*, **87**, 3104 (2005). [DOI: http://dx.doi.org/10.1063/1.2011788]

[11] M. S. Lundstrom and Z. Ren, *IEEE Trans. Electron Devices*, **49**, 133 (2002). [DOI: http://dx.doi.org/10.1109/16.974760]

[12] M. Charmi, H. R. Mashayekhi, and A. A. Orouji, *J. Comput. Electron.*, **13**, 307 (2014). [DOI: http://dx.doi.org/10.1007/s10825-013-0528-x]

[13] M. Charmi, *Chin. Phys. B*, **24**, 047302 (2015). [DOI: http://dx.doi.org/10.1088/1674-1056/24/4/047302]

[14] M. M. Frank, S. B. Kim, S. L. Brown, J. Bruley, M. Copel, M. Hopstaken, M. Chudzik, and V. Narayanan, *Microelectron. Eng.*, **86**, 1603 (2009). [DOI: http://dx.doi.org/10.1016/j.mee.2009.03.063]

[15] H. Lu, W. Y. Lu, and Y. Taur, *Semicond. Sci. Technol.*, **23**, 5006 (2008).

[16] L. Zhang, J. Zhang, Y. Song, X. Lin, J. He, and M. Chan, *Microelectron. Reliab.*, **50**, 1062 (2010). [DOI: http://dx.doi.org/10.1016/j.microrel.2010.04.005]

[17] A. Cerdeira, B. I-iguez, and M. Estrada, *Solid-State Electronics*, **52**, 1064 (2008). [DOI: http://dx.doi.org/10.1016/j.sse.2008.03.009]

[18] A. A. Ziabari, M. Charmi, and H. R. Mashayekhi, *Chines J. Phys.*, **51**, 844 (2013).

[19] K. Suzuki, Y. Kataoka, S. Nagayama, C. W. Magee, T. H. Buyuklimanli, and T. Nagayama, *IEEE T. Electron Dev.*, **54**, 262 (2007). [DOI: http://dx.doi.org/10.1109/TED.2006.888676]

[20] S. M. Sze, *Physics of Semiconductor Devices* (New York, USA, 1983).

[21] S. Karmalkarand and K. N. Bhat, *IEEE J. Solid-St. Circ.*, **24**, 139 (1989). [DOI: http://dx.doi.org/10.1109/4.16313]

[22] G. Zhang, Z. Shaoand, and K. Zhou, *IEEE T. Electron Dev.*, **55**, 803 (2008). [DOI: http://dx.doi.org/10.1109/TED.2007.914832]

[23] R. Venugopal, Z. Ren, S. Datta, M. S. Lundstrom, and D. Jovanovic, *J. Appl. Phys.*, **92**, 3730 (2002). [DOI: http://dx.doi.org/10.1063/1.1503165]

[24] S. Datta, *Superlattices and Microstructures*, **28**, 253 (2000). [DOI: http://dx.doi.org/10.1006/spmi.2000.0920]

[25] S. Datta, *Quantum Transport: Atom to Transistor* (Cambridge, Cambridge University Press, UK, 2005). [DOI: http://dx.doi.org/10.1017/CBO9781139164313]

[26] M. Lundstrom and J. Guo, *Nanoscale Transistors: Device Physics Modeling and Simulation* (Springer Press, USA, 2006).

[27] M. Goano, *Solid-State Electronics*, **36**, 217 (1993). [DOI: http://dx.doi.org/10.1016/0038-1101(93)90143-E]

[28] F. Venturi, R. K. Smith, E. C. Sangiorgi, M. Pinto, and B. A. Ricco, *IEEE Trans. Electron Dev.*, **8**, 360 (1989).